SERS and DFT of 5F-PB-22

Journal:	*Journal of Raman Spectroscopy*
Manuscript ID	JRS-17-0349
Wiley - Manuscript type:	Research Article
Date Submitted by the Author:	01-Dec-2017
Complete List of Authors:	Baron, Mark; University of Lincoln, School of Chemistry Alkaseem, Mohammad; University of Lincoln, School of Chemistry
Keywords:	SERS, DFT, 5F-PB-22, synthetic cannabinoids
Note: The following files were submitted by the author for peer review, but cannot be converted to PDF. You must view these files (e.g. movies) online.	
Figure 1.cdx	

SCHOLARONE™
Manuscripts

SERS and DFT study of 5F-PB-22

Mohammad Alkaseem and Mark Baron

School of Chemistry, University of Lincoln, Brayford Pool, Lincoln, LN6 7TS

Abstract: In this work, a joint experimental and theoretical study on 5F-PB-22 (1-(5-fluoropentyl)-8-quinolinyl ester-1H-indole-3-carboxylic acid) is reported. The molecular vibrations of 5F-PB-22 were investigated by Raman and SERS spectroscopies. In parallel, quantum chemical calculations based on density functional theory (DFT) were used to determine the geometrical and vibrational characteristics of the molecule with emphasis on the interaction and adsorption geometry of the molecule to the silver colloidal surface. The SERS spectrum of 5F-PB-22 was recorded using a 532-nm laser line and hydroxylamine phosphate reduced silver colloid as SERS substrate after developing two-step aggregation procedures by studying the effect of NaCl on the Surface Plasmon Resonance. Raman and SERS spectra of 5F-PB-22 were assigned based on DFT calculations with the hybrid B3LYP exchange-correlation functional, coupled with the standard 3-21G basis set. The calculated molecular electrostatic potential (MEP) was used in conjunction with the SERS data to predict the adsorption geometry of the molecule on the silver surface.

Keywords: SERS, 5F-PB-22, synthetic cannabinoids, DFT

For Peer Review

Introduction

5F-PB-22 also known as 5F-QUPIC, is a quinolinyl carboxylate derivative belonging to the synthetic cannabinoids, but differs from the earlier generation naphthyl indole, AM-2201, by replacing the naphthalene group with an 8-hydroxyquinoline moiety. 5F-PB-22 has the chemical structure of 1-(5-fluoropentyl)-1H-indole-3-carboxylic acid 8-quinolinyl ester as shown in Figure 1 and is a full agonist of the cannabinoid receptors [1]. It first appeared in 2013 and since then has been detected in products obtained from smoke shops, online vendors and retail outlets. Since May 2016, with the introduction of the Psychoactive Substances Act the sale, distribution, imports and purchase of 5F-PB-22 is banned in the UK [2].

The consumption of 5F-PB-22 has been linked to adverse effects including tachycardia, myocardial infarction, convulsions and seizures and it has been implicated in human deaths. It has also been associated with driving impairment cases [3-4]. Thus there is a need for sensitive

methods to detect 5F-PB-22 at the low concentrations (e.g. $\leq 10^{-7}$ M) found in biological fluids [5].

Since the first reported Surface-enhanced Raman spectroscopy (SERS) of pyridine molecules on a silver electrode by Fleischmann et al. in 1974 [6], silver nanoparticles (AgNPs) have become the most commonly used nanostructures for SERS owing to their large enhancement factors with single-molecule detection being successfully achieved on colloidal nanoparticles [7]. Colloidal AgNP can be prepared by different methods, including chemical reduction, photo-reduction, and laser ablation. Chemical reduction is the most frequently applied method for the preparation of AgNPs as stable, colloidal dispersions in water or organic solvents. Commonly used reductants are borohydride, citrate, ascorbate, hydroxylamine and elemental hydrogen. The reduction of silver ions (Ag+) in aqueous solution by hydroxylamine generally yields silver colloids with different properties (particle size, optical properties, stability, etc) depending on the hydroxylamine salt, the method of preparation and the stabilizing agent used. A simple, fast method has been proposed recently by fast injection of silver ions into alkaline hydroxylamine phosphate which produces a stable silver colloid with a shelf life greater than 1 year and a particle size of approximately 20 nm and narrow size distribution [8-10].

It is now generally accepted that the enhancement mechanisms underpinning the SERS effect are either electromagnetic or chemical in origin. The former arises from the optical excitation of surface plasmon resonances (SPRs) at the surface of the metal, which leads to a significant increase in the electromagnetic field strength. The latter is due to changes in the electronic structure of molecule adsorbed on the metal surface, which selectively enhances some Raman peaks. Charge transfer (CT) between the molecule and the SERS-active substrate is typically responsible for the chemical enhancement. Of these contributions to the overall enhancement, SPR is mostly a property of the metal, whereas charge-transfer resonance is a property of the combined metal-molecular system [11]. Nonetheless, the greatest SERS enhancement occurs for molecules adsorbed at electromagnetic hot spots; the gap region between closely spaced silver (or gold) nanoparticles where SPRs are coupled significantly increasing the Local Field Intensity Enhancement Factor (LFIEF). Aggregation of colloidal AgNPs is therefore required to maximise the LFIEF and the SERS response.

Nanoparticle aggregates are of interest since they present many 'hot spots' and produce intense SERS [12]. Chen et al. observed increases in SERS intensity with the degree of AgNP aggregation, using a gas-evaporation method. Variation in the observed enhancement of the Ag aggregated films was attributable to the density of particles and the degree of its "surface roughness" [13]. SERS of a set of structurally similar synthetic cannabinoids has been obtained by mixing the analyte with colloidal gold nanoparticles and alkali or alkaline earth salts. The salts produced an aggregation of the nanoparticles with a resultant spectral enhancement due to the formation of spectral hotspots with enhanced field effects within the aggregate [14].

Mabbott et al observed a color change in AgNPs when they added chloride to generate aggregation to get SERS for eighty different illicit drugs. Their observation is consistent with aggregation as the nanoparticle solution displays a bathochromic shift [15]. Doctor et al. observed the ability of different chloride salts, $MgCl_2$, $CaCl_2$, KCl, and NaCl, to generate SERS of benzodiazepines via aggregation for colloidal gold nanoparticles. However, they found that each

For Peer Review

aggregating agent produced different levels of signal enhancement. An important reason for using aggregation agents is that most molecules are not able to generate complete self-aggregation, or they have a limited contribution to the aggregation process when present at low concentrations [16]. Which may explain the absence of a general aggregating agent for different compounds.

It is noteworthy, that the general SERS procedures for different molecules (synthetic cannabinoids in particular) has been done by adding a specific volume of aggregating agent (≤critical coagulation concentration) to the colloidal nanoparticle followed by a small volume of the analyte (in general at very low concentration) with respect to mixing and equilibrium time in each step [14-17]. To the best of our knowledge, none of the published reports about SERS of synthetic cannabinoids has considered the effect of the aggregating agent on SPR, the self-aggregation of the target molecules, using a two-step aggregation procedure, and the orientation of the molecule on the surface of the nanoparticles. A direct relation between aggregation and SERS enhancement, which is empirically based, can facilitate the identification of the molecules through interpreting vibrational modes in the resulting spectra using computational methods such as density functional theory (DFT) or molecular electrostatic potential map (MEP).

There is a lack of analytical research information available on 5F-PB-22 since it is relatively new to the market and consequently has not yet been fully characterized. DFT has recently become an efficient tool for the prediction of molecular structure, vibrational wavenumbers, IR and Raman activities of any compound of interest. These methods predict relatively accurate molecular structure and vibrational spectra with moderate computational effort. Comparisons of the results from DFT theory with the results of experiments have shown that the methods using Becke's theory parameter hybrid functional (B3) with correlation functions such as the one proposed by Lee, Yang, and Parr (LYP) are most promising in providing correct vibrational wavenumber assignments [18-19].

In the present study, SERS and Raman spectra of 5F-PB-22 were assigned using DFT calculations based on the hybrid B3LYP exchange-correlation functional, coupled with the standard 3-21G basis set. A modified SERS procedure has been developed by adopting a two-step aggregation using NaCl and the adsorption geometry of the 5F-PB-22 molecule on the colloidal silver surface was deduced from the SERS selection rules and the analysis of the calculated molecular electrostatic potential (MEP).

Experimental

Chemicals and materials

5F-PB-22 was purchased from the internet (Ravebeans.com), in September 2014, the label claimed that the purchased compound is GC/MS grade and has purity 99.5%, Identity and purity of the purchased compound were confirmed before use. Silver nitrate (99.9999%, metals basis, Sigma-Aldrich), hydroxylamine phosphate ($(NH_2OH)_3 \cdot H_3PO_4$, 97%, Aldrich), sodium chloride (>99.5%, BDH), sodium hydroxide (>97%, Fisher Scientific), 18 MΩ deionised water was used for preparation of solutions. All other chemicals used were obtained from Sigma-Aldrich (St. Louis, MO) and used without further purification.

Preparation of hydroxylamine phosphate silver colloid and SERS

Hydroxylamine phosphate silver nanoparticles (HPAg) were prepared following the procedure outlined by White and Hjortkjaer [10]. An aqueous solution of hydroxylamine phosphate (100 µl; 0.077 M) was added to an aqueous solution of sodium hydroxide (4.5 ml; 3.33×10^{-3} M) in a 7.5 ml polystyrene vial (Sterelin), capped and inverted slowly three times. After 30 s, an aqueous solution of silver nitrate volume (500 µl; 10^{-2} M) was introduced rapidly into the mixture in less than 0.5 s by using a 1 ml Eppendorf pipette and a 1 ml disposable tip (Fisherbrand) held 1 cm above the liquid surface. The capped vial was then inverted very slowly through 180° and back again 15 times in 60s.

The 5F-PB-22 samples for UV-Vis and Raman analysis were prepared by spiking 5F-PB-22 into 0.480 mL of colloid to have a concentration in the range 1.07×10^{-3} to 1.06×10^{-7} M without changing the total volume (0.5 mL) or the concentration of the nanoparticles as illustrated in Table S1 (Supporting Information). Samples for studying the effect of NaCl concentration on the SPR were in the range from 0-100 mM and are shown in Table S2 (Supporting Information).

Instrumentation

Identification of 5F-PB-22 was done using the mid-infrared spectrum of 5F-PB-22 powder recorded directly on a Golden Gate Attenuated Total-internal Reflection (ATR) accessory (Specac) housed in a Perkin-Elmer Spectrum 100 Fourier Transform Infrared Spectrometer (FTIR) equipped with a DTGS detector. Spectra were recorded at a scan speed of 0.2 cm/s, 64 scans, and resolution of 4 cm^{-1}. The obtained spectra were compared with the 5F-PB-22 spectrum in the SWG-Drug Library (Version 4).

Further confirmation of the identity and purity was done by direct infusion of a 5F-PB-22 methanol solution into a high-resolution, accurate-mass (HR/AM) Thermo Scientific™ Exactive™ Plus Orbitrap Mass Spectrometer. Fragmentation pattern was obtained using a scan range 50-500 m/z, resolution 70.000, positive polarity, a micro scan of 1, $1e^6$ of AGC target, 3.80 kV spray voltage. The fragmentation of the purchased compound correlated to the fragmentation pattern of 5F-PB-22 to confirm the identity.

UV/visible spectroscopy absorption spectra of the colloid were obtained on a Shimadzu UV/visible 1800 PC spectrophotometer over a wavelength range of 300–600 nm or 250-900 nm with a sampling interval of 0.5 nm (fast scan). UV/visible spectra of colloidal solutions were obtained by pipetting 60 µl of the colloid into 4 ml disposable polystyrene cuvettes (Sarstedt) and adding 3 ml of water (characterization of the prepared nanoparticles). SERS-samples were diluted by the ratio 1:10 with water in Quartz cuvettes for UV-Vis measurements. Particle size and Zeta potential measurements were performed with a Malvern Zetasizer Nano ZS (Malvern, Herrenberg, Germany) equipped with a 633 nm He-Ne laser and operating at an angle of 173º. The software used to collect and analyze data was the Dispersion Technology software version 6.01 from Malvern. 500 µl of sample was pipetted into a single-use polystyrene cuvette (Fisher Emergo, Landsmeer, The Netherlands) with a pathlength of 10 mm. The measurements were made at the position of 4.65 mm from the cuvette wall with an automatic attenuator and at a controlled temperature of 25 ºC. For each colloid batch, 15 runs of 10s were performed. The size

For Peer Review

average and polydispersity index (PDI) were obtained from an auto-correction function using the "general purpose mode" for all batches.

Nanoparticle tracking analysis (NTA) was performed with a Nanosight LM20 (NanoSight, Amesbury, United Kingdom), equipped with a sample chamber with 532 nm green laser and a Viton fluoroelastomer O-ring. The sample chamber was filled with colloid using sterile syringes (BD Discarded, New Jersey, USA). All the measurements were performed at room temperature. The software used for capturing and analyzing the data was the NTA 2.0 build 127. The sample was measured for 1 minute with a manual shutter and gain adjustments.

Raman and SERS spectra were recorded using a LABRAM 300 (Horiba Jobin Yvon) with an excitation line of 532 nm. The instrument was equipped with an Olympus microscope BX41, which was used to collect Raman spectra from the powder using a 50×, 0.50 NA Leica objective with a long working distance that focused the laser onto the surface of the powder. A sample holder was employed for glass cuvettes (0.5 cm path length), used to analyse liquid samples. In all the experiments, an output power of 50mW, 5 s of exposure time, and 2 accumulations were used. SERS samples were prepared as described previously for UV-Vis with aggregation induced by different concentrations of NaCl (10-100 mM) added before and/or after the addition of 5F-PB-22 to the HPAg colloid.

For Peer Review

Computational details

The molecular geometry optimization, molecular electrostatic potential (MEP) and vibrational spectra calculations were performed with the Gaussian9w package using DFT methods with the B3LYP hybrid exchange-correlation functional and split valence plus polarization 3-21G basis sets to predict the Raman spectra of 5F-PB-22. No symmetry restriction was applied during geometry optimization. The vibrational wavenumbers were computed at the optimized geometry to ensure that no imaginary wavenumbers were obtained confirming that it corresponds to a local minimum on the potential-energy surface. The computed wavenumbers have been scaled by 0.965 as proposed by NIST Computational Chemistry Comparison and Benchmark Database. Mode assignment is based on Gauss View 5 and VEDA as well as a direct comparison between the experimental and calculated spectra by considering both the wavenumber sequence and intensity pattern [20-22].

Results and discussion

Confirmation of identity and purity of 5F-PB-22

FTIR results show that the unique collection of absorption bands in the spectrum of purchased compound was consistent with the 5F-PB-22 chemical structures and in line with the 5F-PB-22 spectrum in the SWG Drug Library (Version 4) as shown in Fig S1 (Supporting Information).

The identification and the purity of the purchased compound was further confirmed using high-resolution, accurate-mass (HR/AM) mass spectrometry. The EI fragmentation peaks for the purchased compound are reported in Fig S2 (Supporting Information) as m/z (% abundance) for peaks ≥1% abundance. The predicted fragmentation pattern of 5F-PB-22 shown in Fig S3

(Supporting Information) is consistent with the experimental results, where all the fragments (m/z) with ≥1% abundance of the purchased compound are related to 5F-PB-22 structure. Thus, no further tests were done, and the identity of the purchased compound was confirmed as 5F-PB-22 with a good purity determined by the fragment patterns and relative abundances to the main ion.

Characterisation of phosphate-capped silver nanoparticles

The hydroxylamine phosphate silver nanoparticles (HPAg) used in this study were prepared adopting a previously reported procedure for reproducible preparation of silver colloid with strong SERS properties by the reduction of silver nitrate with hydroxylamine phosphate [10]. 10 batches were prepared and characterized by UV/Vis spectroscopy, dynamic light scattering (DLS), nanoparticle tracking analysis (NTA) and zeta potential as shown in Figure 2**.** The pH of the 24-hour aged colloid was 7.6±0.2 and the resultant nanoparticles ranged in size from 10 to 100 nm with an average size (Z-ave) of 38.50 nm with a polydispersity index (PDI) of 0.146, and a zeta potential of -36±1.5 mV. The absorption spectra of all prepared samples showed a surface plasmon peak at a wavelength of 396.3±1.76 nm with absorbance 0.281±0.012 and a bandwidth at half height of 56.6±4.14 nm. NTA results give a particle size of 35 nm with a concentration of 9.18×10^{11} particle/ml This is consistent with the spherical cluster approximation [23], assuming that, the prepared nanoparticles are spherical [10] with an average size of 38.50 nm (zeta sizer), the total number of nanoparticles was 4.056×10^{11} per mL, the calculated concentration of the nanoparticles found = 6.73 x 10^{-7} M (see calculation of nanoparticle concentration, Supporting Information). The surface plasmon peak wavelength, absorbance, and bandwidth are in good agreement with White & Hjortkjaer, with a small difference in the nanoparticle size which may be related to the speed of injection of the silver nitrate solution into the sodium hydroxide-hydroxylamine mixture during the manual preparation of the colloid. A zeta potential greater than -30 mV, indicates a stable colloid and is in agreement with the results proposed by White & Hjortkjaer who found, that HPAg colloids were stable for more than a year.

The effect of different concentrations of sodium chloride (0-100 mM) on the surface plasmon peak of the prepared HPAg was studied.

Figure 3 shows the UV-Vis absorbance spectra changes of HPAg along with increasing the concentration of NaCl from 0 mM to 100 mM. The absorbance at 396.3 nm decreases with the increase of NaCl concentration. The aggregation of HPAg is indicated by a decrease in the absorption of 396.3 nm band and the appearance of a second band in the region 700-900 nm when using NaCl at a concentration of 20 mM. The small red shift of the absorption maximum with an increase in ionic strength (> 10 mM NaCl) suggests increased particle size and aggregation tendency, which may result from forming larger clusters of nanoparticles, according to the Derjaguin, Landau, Verwey, and Overbeek (DLVO) theory [24]. The DLVO theory represents the interaction potential as a superposition of van der Waals and electric double-layer forces and explains why colloids are stable at low salt levels, and unstable at higher salt levels. According to DLVO theory and as observed in the UV-Vis results, at low NaCl levels (≤ 10 mM), the repulsive double-layer forces dominate and lead to slow aggregation. At higher NaCl levels (≥20 mM), double-layer forces are screened, and the attractive van der Waals forces induce fast aggregation in which cluster-cluster interactions dominate resulting from the partial

removal of surface charges [25]. NaCl concentrations of 10, 20, 40 and 100 mM were chosen for further investigation.

Normal Raman, SERS, and DFT calculation

Raman spectrum of 5F-PB-22 was obtained at excitation wavelength of 532 nm. Figure 4 shows that the obtained spectrum was not affected by background fluorescence emission across the spectral range (200-4000 cm^{-1}).

Figure 5 illustrates that at concentrations < 7.4×10^{-4} M of 5F-PB-22, the only remarkable peak observed in normal Raman spectra is at ~ 1035 cm^{-1}, which can be assigned to the Raman C – O stretching mode of methanol [27].

SERS spectra were obtained at a concentration of 5F-PB-22 from 7.4×10^{-4} M to 1.076×10^{-3} M with the most intense peaks at 1363.8 cm^{-1}, followed by peaks at 1565.4, 726.1 and 497.4 cm^{-1} respectively.

The onset of SERS (when the concentration of 5F-PB-22 reached a 7.4×10^{-4} M) indicates some changes in the solution. UV-visible spectra (Figure 6) of the SERS samples show a peak in the region 700-900 nm, along with decreasing intensity of the SPR band of HPAg at 396.3 nm and a small red shift. The red shift of 396.3 nm peak as 5F-PB-22 up to 6.36×10^{-4} M may be explained according to Mie theory by the extinction cross section changing by coating the nanoparticles with 5F-PB-22[28-30]. However, a further increase in [5F-PB-22] brings the nanoparticles close enough to form dimers or higher aggregates shown by the appearance of the peak at 750 nm. Spectral changes due to aggregation are supported by the decrease of zeta potential value from -36mV of pure nanoparticles to -18 and -2.08 mV when the concentration of 5F-PB-22 reaches 6.36×10-4 M and 7.4×10-4 M respectively. The change in zeta potential value happens as the ratio of 5F-PB-22 molecules to the total number of nanoparticle-surface atoms reaches a value of approximately 2. This explains the weak effect of lower concentration (< 6.36×10-4) on zeta potential and SPR as there are insufficient molecules to cover all the nanoparticle-surface atoms (see, Calculation of 5F-PB-22 molecules number coating nanoparticle-surface atoms, Supporting Information).

Commingling Raman and UV-Vis results may suggest that the aggregation of the nanoparticles and the onset of SERS are closely parallel. As can be observed in Figure 6, the SPR is shifted and becomes closer to the laser line (532 nm), in addition to the onset of SERS and the appearance of the peak in the range of 700-900 nm appear nearly concurrently which appears to drive the activation of SERS in the (HPAg,5F-PB-22) system. It was noticeable that the SERS activity appears when the absorbance declines from its maximum value to a critical value after which a small addition of 5F-PB-22 is enough to generate SERS. The absorbance decline at this point is comparable to the effect of adding NaCl in a concentration of 10 mM (Figure 3) and suggests that 10mM NaCl can be used as a trigger for aggregation as well as using NaCl concentrations in the range 20-100 mM to generate complete aggregation.

A set of experiments, wherein aggregation was applied before and after the addition of 5F-PB-22 to the nanoparticles solutions were performed to examine the possibility of observing SERS spectra at concentrations below those at which 5F-PB-22 itself appears to trigger the SERS as described previously.

For Peer Review

Figure 7 shows that, when a single spike was used to increase [5F-PB-22] to 1.06×10^{-7} M, SERS was not observable however, following addition of 100 mM NaCl, a strong mode was immediately observed to appear at around 236.1 cm^{-1}. When NaCl was added before 5F-PB-22 a concentration > 20 mM yielded a strong mode at 236.1 cm^{-1} that masks the 5F-PB-22 spectrum. As little as 1.06×10^{-7} M 5F-PB-22 is not sufficient to drive self-aggregation of nanoparticles and using NaCl for aggregation at a concentration higher than 20 mM has not been useful for SERS. However, the addition of a lower concentration of NaCl at10mM, followed by 1.06×10^{-7}M 5F-PB-22, and finished with [NaCl] at either 20 or 40 mM yielded the most intense SERS. Using 10 mM NaCl and finished with 20 mM NaCl appears to give the strongest 5F-PB-22 SERS and the weakest AgCl SERS. A similar result is obtained at 2.12×10^{-8} M 5F-PB-22.

The previous results could be explained by the fact that the appropriate aggregation of the nanoparticles will form nano-junctions between two plasmonic surfaces, which would generate SERS "hotspots" [31]. However, these "hotspots" usually exist at the nanogaps between the nanoparticles with rough surfaces and a random arrangement. Therefore, nanogaps are the key to obtaining strong SERS. The nanogaps seem to be more uniform when the aggregation is triggered with a small quantity of sodium chloride, rather than excessive aggregation induced by a high concentration of sodium chloride. The changes in UV-Vis properties of the nanoparticles indicate the formation of aggregates to form nanogaps and "hotspots" giving much stronger SERS signals [32]. Experimentally, it was found that the SERS of 5F-PB-22 is negatively correlated with the formation of extended aggregates as silver colloid slowly precipitates due to the formation of large clusters of silver particles. With gradual precipitation of larger clusters, fewer clusters are available for SERS, which explains the decrease in the SERS observed when collecting Raman spectra after 2 hours. In contrast to Figure 6 where absorbance declines with increasing concentration of 5F-PB-22, Figure 8 shows an increase in absorbance when using NaCl before the addition of 5F-PB-22 to the colloid. This result may suggest a role of NaCl in re-orientation of the 5F-PB-22 molecule in a way which helps the adsorption of the molecule on the surface of nanoparticles.

To better understand the SERS activity of 5F-PB-22 and the effect of low concentration of NaCl on triggering SERS, the optimized geometrical parameters, Raman activity, molecular electrostatic potential (MEP) and vibrational spectra were calculated for 5F-PB-22. In addition, spectra of 8-hydroxyquinoline and 1-(5-fluoropentyl)-1H-indole-3-carboxylic acid which result from the dissociation of 5F-PB-22 as seen in Fig S4 (Supporting Information) were calculated using the DFT/ B3LYP (3-21G). The optimized geometrical structure of 5F-PB-22 obtained by the bond length and bond angle values is given in Table 1. It is important to mention that the indole ring and quinolinyl ring are located in perpendicular levels as shown in Figure 9.

DFT results show that the optimized geometrical structure of 5F-PB-22 has C1 point group symmetry with 141 fundamental modes of vibrations (3N-6) distributed into 48 stretching modes, 47 bending modes, 46 torsion modes without observing any imaginary wavenumbers. The experimental and calculated wavenumbers are scaled by the factor 0.965 and summarized in Table 2.

Figure 10 shows Raman, SERS and DFT-calculated spectra of 5F-PB-22, as well as DFT calculated spectra of 8-hydroxyquinoline and 1-(5-Fluoropentyl)-1H-indole-3-carboxylic acid. SERS spectra of 5F-PB-22 collected with and without the addition of NaCl show that NaCl produces some spectral shifts with substantial re-distribution of mode intensities which might

For Peer Review

explain how NaCl promotes the orientation. New modes appear at around 1716, 707.3, 1013, and 1529 cm^{-1}, as well as changes in the relative intensities of the modes at 770, 1096 and 1339 cm^{-1}, taking into account that the mode at 236 cm^{-1} is associated with NaCl and is dependent on the presence of 5F-PB-22.

DFT-calculated spectrum of 8-hydroxyquinoline shows a very strong mode at around 1337 cm^{-1}, which appears as a strong mode at 1332 cm^{-1} in the calculated spectrum of 5F-PB-22 and in the normal Raman spectrum. However, this mode appears as a very weak mode at 1339 cm^{-1} in the SERS spectrum. The medium modes at 1535 and 1044 cm^{-1} in the calculated 8-hydroxyquinoline spectrum are shifted to 1446 and 1041 cm^{-1} in the calculated spectrum of 5F-PB-22 and its normal Raman spectrum, but are absent in the SERS spectrum. These three modes are assigned to CC stretching modes in the quinoline ring. Similar results were observed for the modes at 582, 1411, 1440, and 1615 cm^{-1} which all are assigned to the contribution of the quinolinyl moiety in the Raman spectrum of 5F-PB-22. Previous results suggest that the 8-hydroxyquinoline contribution in SERS spectra is very weak.

DFT-calculated spectrum of 1-(5-fluoropentyl)-1H-indole-3-carboxylic acid shows a strong mode at around 1362 cm^{-1}, which appeared as a medium mode at 1361 cm^{-1} in the calculated spectrum of 5F-PB-22, and as a very strong mode at 1362 cm^{-1} in the SERS spectrum.

The very strong mode at 1698 cm^{-1} is assigned to CO stretching in the calculated spectrum, shifted to 1718 cm^{-1} in the calculated spectrum of 5F-PB-22 and appeared as a medium band in SERS and disappeared in the spectrum of 5F-PB-22 driven by self-aggregation without NaCl. Similar findings were observed for the modes at around 1011, 769, 723, 1562 cm^{-1} in the SERS spectrum (Figure 10), which are all assigned to the contribution of 1-(5-fluoropentyl)-1H-indole-3-carboxylic moiety in the SERS spectrum.

The previous discussion suggests that the contribution of quinolinyl moiety in SERS spectrum is weak and the main features of the SERS spectrum are generated mainly from 1-(5-fluoropentyl)-1H-indole-3-carboxylic moiety. Theoretically, the interaction of 5F-PB-22 with the silver surface can be established through the electron pairs of the O and N, as well as through the π –electrons of the rings. The adsorption of 5F-PB-22 to the silver surface is deduced based on the molecular electrostatic potential map and several marker bands as discussed above. Figure 11 shows the calculated 3D electrostatic potential contour map of 5F-PB-22 in atomic units with the electron density isosurface being 0.02 a.u. According to the SERS surface-selection rules, the normal modes, with a change in polarizability component perpendicular to the surface, are enhanced. As seen in Figure 11 the highest electron density is located on oxygen atoms, thus the molecule can interact through this group (CO) with the silver surface. Considering previous discussion, the quinolinyl moiety appears to lie in a preponderant parallel orientation to the silver surface. The intense Raman bands at 1332 cm^{-1}, assigned to the quinoline ring, are present only as a very weak band at 1339 cm^{-1} in the SERS spectrum. Also, the bands due to CC stretching vibrations from quinolinyl moiety are absent. The very strong intensity of the NC stretching band (1362 cm^{-1}), indicate that this group lies in the proximity of the silver surface. Also, intense bands in the SERS spectrum are observed at 1011, 769, 723, 1562 cm^{-1} pointing to the adsorption of the 5F-PB-22 molecule through the O atom to the silver surface.

Previous discussion suggests that 5F-PB-22 has potential to drive nanoparticle-nanoparticle interaction via intermolecular forces (e.g via H-bonding) at a concentration of 10^{-5} M, however at lower concentration, NaCl is needed to promote the aggregation, where Cl^- will associate with

For Peer Review

the nanoparticle surfaces, possibly displacing some of the capping agent (phosphate) and when 5F-PB-22 is added to this solution will adsorb onto the nanoparticle surface and reduces the repulsive forces between the nanoparticles promoting a limited aggregation. Subsequent addition of NaCl can cause the entrapment of 5F-PB-22 molecules in the junction between the particles "hot spot" which will produce the largest SERS signal. If the initial concentration of NaCl is high large aggregates will form with their surfaces saturated by Cl^- which prevents 5F-PB-22 from adsorption onto the surface and hence prevents SERS.

Conclusions

The results demonstrate that, in 5F-PB-22 SERS experiments, it is important to optimise NaCl concentration and the SERS procedure itself in order to obtain intense SERS using phosphate-capped silver nanoparticles. It was found that sodium chloride affects the SPR and, consequently the SERS signal, when it is used to promote a limited aggregation prior to adding the analyte. The findings show that further aggregation after adding the analyte is another crucial factor to obtain intense SERS. This work shows the effect of NaCl, at low concentration, on local surface plasmon resonance and the benefit of using a two-step aggregation process to produce high intensity SERS. It was found that 10mM NaCl can be used as a trigger for aggregation before adding 5F-PB-22 where complete aggregation could be achieved easily using 20-100 mM. It was shown that the optimized geometrical structure of 5F-PB-22 (DFT/B3LYP/3-21G) has C1 point group symmetry with 141 fundamental modes of vibration that were used for interpretation of the SERS spectrum. The calculated 3D electrostatic potential contour map shows the highest electron density located on the oxygen atom of the carbonyl group. This result combined with the SERS selection rules provides an orientation of the 5F-PB-22 molecule on the nanoparticle surface. The quinolinyl moiety in 5F-PB-22 lies in a preponderant parallel orientation to the silver surface with a poor contribution to the SERS spectrum which is generated mainly from the 1-(5-fluoropentyl)-1H-indole-3-carboxylic moiety and the carbonyl group

Acknowledgments

Authors would like to thank Council for At-Risk Academics (CARA) and Lincoln University for all the support they provide to this work.

References

[1] S. D. Banister, J. Stuart, R. C. Kevin, A. Edington, M. Longworth, S. M. Wilkinson, C. Beinat, A. S. Buchanan, D. E. Hibbs, M. Glass, M. Connor, I. S. McGregor, M. Kassiou, *ACS Chem. Neurosci*. **2015**, http://dx.doi.org/ 10.1021/acschemneuro.5b00107

[2] Psychoactive Substances Act **2016**. www.legislation.gov.uk. Retrieved 2016-05-25

[3] S. M. R. Gurney, K. S. Scott, S. L. Kacinko, B. C. Presley, B. K. Logan, *Forensic Sci Rev*. **2014**

[4] T. Jordan, R. R. R. Gerona, M. D. Schwartz, *N. Engl. J. Med*. **2015**. http://dx.doi.org/10.1056/NEJMp1505328

For Peer Review

[5] A. A. Aldlgan, , *TrAC, Trends Anal. Chem.* **2016**, 80, 444-457. https://doi.org/10.1016/j.trac.2016.03.025

[6] M. Fleischmann, P. A. Hendra, A. McQuillan, *J.Chem.Phys.Lett*. **1993**, 26, 163.

[7] M Cyrankiewicz, T Wybranowski, S Kruszewski, *J. Phys.: Conf. Ser*. **2007**, 79 - 012013

[8] S. Bekkeri,*IOSR J. Pharm*.**2013**; 4, 7, http://dx.doi.org/10.9790/3013-0407038044

[9] A. Campion, P. Kambhampati, ***Chem. Soc. Rev.***, 1998,**27**, 241-250, http://dx.doi.org/10.1039/A827241Z

[10] P. White, J. Hjortkjaer, *J. Raman Spectrosc*. **2014**, 45, 32–40. http://dx.doi.org/10.1002/jrs.4412

[11] E. C. Le Ru, P. G. Etchegoin, *Principles of Surface Enhanced Raman Spectroscopy and Related Plasmonic Effects*, Elsevier, Amsterdam, 2009.

[12] T. A. Laurence, G. Braun, C. Talley, A. Schwartzberg, M. Moskovits, N. Reich, T. Huse, *J. AM. CHEM. SOC*. **2009**; 131. 162–169, http://dx.doi.org/ 10.1021/ja806236k

[13] M. C. Chen, S. D. Tsai, M. R. Chen, S. Y. Ou, W. H. Li, K. C. Lee, *Phys. Rev. B*. **1995**; 51, 4507.

[14] T. Mostowtt , Talanta. 2017; 164, 396–402. https://doi.org/10.1016/j.talanta.2016.11.002

[15] S. Mabbott, E. Correa, D.P. Cowcher, J.W. Allwood , R. Goodacre, *Anal. Chem*. **2013**; 85, 923−931. http://dx.doi.org/ 10.1021/ac302542r

[16] E. L. Doctor, B. McCord, *Analyst*. **2013**; 138, 5926–5932. http://dx.doi.org/ 10.1021/10.1039/c3an00669g

[17] C. Muehlethaler, M. Leona, J. R. Lombardi , *Forensic Sci. Int*. **2016**;268, 1–13.

[18] A. D. Becke, *J. Chem. Phys*. **1993**; 98, 5648.

[19] R. A. Kendall, T. H. Jr. Dunning, R. J. J. Harrison, *Chem. Phys*. **1992**; 96, 6796–6806.

[20] W.H. Hehre, L. Radom, P.v.R. Schleyer, J.A. Pople, *Ab Initio Molecular Orbital Theory* , Wiley, New York, **1986**.

[21] M. J. Frisch, G. W. Trucks, H. B. Schlegel, G. E. Scuseria, M. A. Robb, J. R. Cheeseman, G. Scalmani, V. Barone, G. A. Petersson, H. Nakatsuji, X. Li, M. Caricato, A. Marenich, J. Bloino, B. G. Janesko, R. Gomperts, B. Mennucci, H. P. Hratchian, J. V. Ortiz, A. F. Izmaylov, J. L. Sonnenberg, D. Williams-Young, F. Ding, F. Lipparini, F. Egidi, J. Goings, B. Peng, A. Petrone, T. Henderson, D. Ranasinghe, V. G. Zakrzewski, J. Gao, N. Rega, G. Zheng, W. Liang, M. Hada, M. Ehara, K. Toyota, R. Fukuda, J. Hasegawa, M. Ishida, T. Nakajima, Y. Honda, O. Kitao, H. Nakai, T. Vreven, K. Throssell, J. A. Montgomery, Jr., J. E. Peralta, F. Ogliaro, M. Bearpark, J. J. Heyd, E. Brothers, K. N. Kudin, V. N. Staroverov, T. Keith, R. Kobayashi, J.

For Peer Review

Normand, K. Raghavachari, A. Rendell, J. C. Burant, S. S. Iyengar, J. Tomasi, M. Cossi, J. M. Millam, M. Klene, C. Adamo, R. Cammi, J. W. Ochterski, R. L. Martin, K. Morokuma, O. Farkas, J. B. Foresman, and D. J. Fox, Gaussian 09, Revision A.02, Gaussian, Inc., Wallingford CT, 2016.

[22] M.H. Jamróz, *Spectrochim. Acta, Part A*. **2013**;114, 220–230.

[23] R. L. Johnston, *Atomic and molecular clusters*, Taylor & Francis, London and New York, **2002**.

[24] K. Ueno, M. Watanabe, *Langmuir*, **2011**; **27**, 9105–9115

[25] W. B. Russel, D. A. Saville, W. R. Schowalter, *Colloidal Dispersions*, Cambridge University Press, Cambridge, **1989**

[26] Y. Sun, R. Zheng, Q. Shi, *J. Phys. Chem. B*, **2012**; *116* (15), 4543–4551

[27] H.A. Hushvaktov, F.H. Tukhvatullin, A. Jumabaev, U.N. Tashkenbaev, A.A. Absanov , B.G. Hudoyberdiev , B. Kuyliev, *J. Mol. Struct*, **2017**;1131 ,25-29.

[28] Wustholz, K. L.; Henry, A.-I.; McMahon, J. M.; Freeman, R. G.; Valley, N.; Piotti, M. E.; Natan, M. J.; Schatz, G. C.; Van Duyne, R. P. Journal of the American Chemical Society 2010, 132, 10903–10.

[29] Mie, G. Ann. Phys. Weinheim, Ger. 1908, 25, 377.

[30] Xie, W.; Su, L.; Shen, A.; Materny, A.; Hu, J. Journal of Raman Spectroscopy 2011, 42, 1248–1254.

[31] Z.C. Cai, C.G. Tian, L. Wang, W. Zhou, B.L. Wang, H.G. Fu, *J. RamanSpectrosc*.**2011**;42, 5–11.

[32] W. Xia, J. Sha, Y. Fang, R. Lu, Y. Luo, Y. Wang, Langmuir **2012**; 28, 5444−5449

Table 1; Optimized geometrical of 5F-PB-22 obtained by B3LYP/3-21G, density functional theory calculations

Bond Angle	Value (Å)	Bond length	Value (Å)
C2-C1-C5	108.5061	C1-C2	1.4019
C2-C1-C15	125.7728	C1-C5	1.374
C5-C1-C15	125.7211	C1-C15	1.5399
C1-C2-C3	107.9753	C2-C3	1.3623
C1-C2-C14	130.0035	C2-C14	1.391
C3-N4-C6	126.4286	C3-N4	1.4583
C2-C3-N4	107.0516	C3-C11	1.39
C5-N4-C6	126.5466	N4-C5	1.3495
C1-C5-N4	109.4423	N4-C6	1.07
C1-C5-H28	125.2719	C5-H28	1.47
N4-C5-H28	125.2858	C6-C7	1.5401

For Peer Review

N4-C6-C7	109.4759	C6-H29	1.07
N4-C6-H29	109.4922	C6-H30	1.07
N4-C6-H30	109.4479	C7-C8	1.5401
C1-C15-O16	119.989	C10-F49	1.35
C1-C15-O17	120.0088	C15-O16	1.43
O16-C15-O17	120.0022	C15-O17	1.2585
C18-C22-N26	120.4033	O16-C18	1.4298
C23-C22-N26	120.1628	C18-20	1.3576
D(15,16,18,22)	89.7815	C9-C10	1.5401
D(1,2,14,13)	-0.0466	C18-C22	1.3998
D(1,2,14,42)	-0.0499	C22-N26	1.3418
D(3,2,14,13)	179.9504	C19-C21	1.4052
D(2,3,4,5)	0.0159	C19-H43	1.07
D(2,3,4,6)	-179.9802	C20-H44	1.07
D(11,3,4,5)	-179.9897	C21-C23	1.3991
D(11,3,4,6)	0.0142	C21-H45	1.07
D(16,18,20,44)	-0.1105	C22-C23	1.3935
D(22,18,20,19)	-0.0969	C23-C24	1.3934
D(22,18,20,44)	179.9043	C24-C25	1.3515
D(16,18,22,23)	-179.8674	N26-C27	1.3015

Table. 2 Experimental vibrational observed and calculated wavenumbers, Raman activity and possible vibrational assignment of 5F-PB-22

Calculated at B3LYP/3-21G		Experimental		Possible assignment
scaled	Activity	Δ_{Raman} cm^{-1}	SERS	
239.0	1.0187	235.7	-	C3C11C12C13 TORS+ N4C2C11C3 OUT OF PLANE
311	1.8813	310.1	-	C10C9C8 BEND+ C8C7C6 BEND +N4C3C11 BEND+ F49C10C9 BEND
413	1.3161	411.9	-	C15C1 stretching + O17C15O16 BEND+ N4C3C11 BEND
437	5.5993	436.4	-	C27N26C22C18 TORS+ C25C27N26C22 TORS
455	4.742	-	-	C22C18O16 BEND+ N4C2C11C3 OUT
471	2.9910		-	C27N26C22 BEND+ C22C18O16 BEND+C23C21C19 BEND
496	6.3782	495.9	495.9	Y C=C-C (QUIN)
541	9.374	544.6	455.6	C3C11C12 Scissoring+ C6N4C5 Scissoring
558	11.8321	556.0	556	C3C11C12 IN-PLANE BEND+ C19C20C18 BEND
583	6.8591	580.0	580	C3C11C12C13 TORS+C23C21C19C20 TORS
634	3.3228	631.8	631.8	C13C12C11 BEND

For Peer Review

693	26.9256	706.1	709	C24C25C27 TORS
783	31.42	773.3	770	H45C21C23C22 TORS
848	2.4297	850.5	849.1	H28C5C1C2 TORS
875	1.095	875.0	-	N26C18C23C22 OUT-OF-PLANE
936	53.5961	932.0	-	O16C15 STRE+O17C15O17 BEND+ N26C18C23C22 OUT OF PLANE+ C22C20C16C18 OUT OF PLANE+ C22C20O16C16 OUT
1005	4.8791	1013	1013.5	H41C13C14C2 TORS+ H42C14C13C12 TORS
1041	12.1966	1038.7	-	H44C20C19 BEND
1076	38.4476	1073.6	-	C24C25C27 BEND
1092.8	22.8317	1090.0	1189	N4C5 STRE+ C2C14C13 BEND
1143	36.2266	1150.0	1140.7	C13C14 STRE
1158	31.3188	1162.2	1163	H28C5C1 BEND
1193	27.0019	1192.0	-	N26C22 STRE
1217	11.167	1217	1219	H37C10F49 BEND
1249	22.6064	1245.9	-	C20C18 STRE
1298	24.8776	1295.0	-	H45C21C23 BEND+ H46C24C25 BEND
1332	147.2923	1334.8	1339	C23C21C19 BEND
1363	41.13	1363	1362	N4C3 STRE
1381	43.0814	1380.8	-	H48C27N26 BEND
1435	20.6823	1425.3	-	H48C27N26 BEND
1477	29.3723	1466.7	1463	C11C12 STRE+ C14C13 STRE
1489	91.6731	1488.2	1485	H30C6H29 BEND+ H32C7C31
1529	64.8058	1529.6	1529.6	N26C27 STRE+ C19-C20 STRE+H38C10H37 STRE
1570	8.5467	1572.5	-	C24C25 STRE
1718	244.7964	1712.6	1714	O17C15 STRE
2939	116.2032	2922.7		C7H31+C9H32 STRE
2952	17.2011	2947.8		C7H32 STRE
2978	48.8728	2977.9		C7H32 STRE
3067.1	95.3369	3067.1		C27H48 STRE
3083	142.4699	-		C12H40 STRE

For Peer Review

3099	175.0081	3100.0		C19H43 STRE
3124	96.1257	3124.0		C20H44 STRE
3191	42.3141			C5H28 STRE

For Peer Review

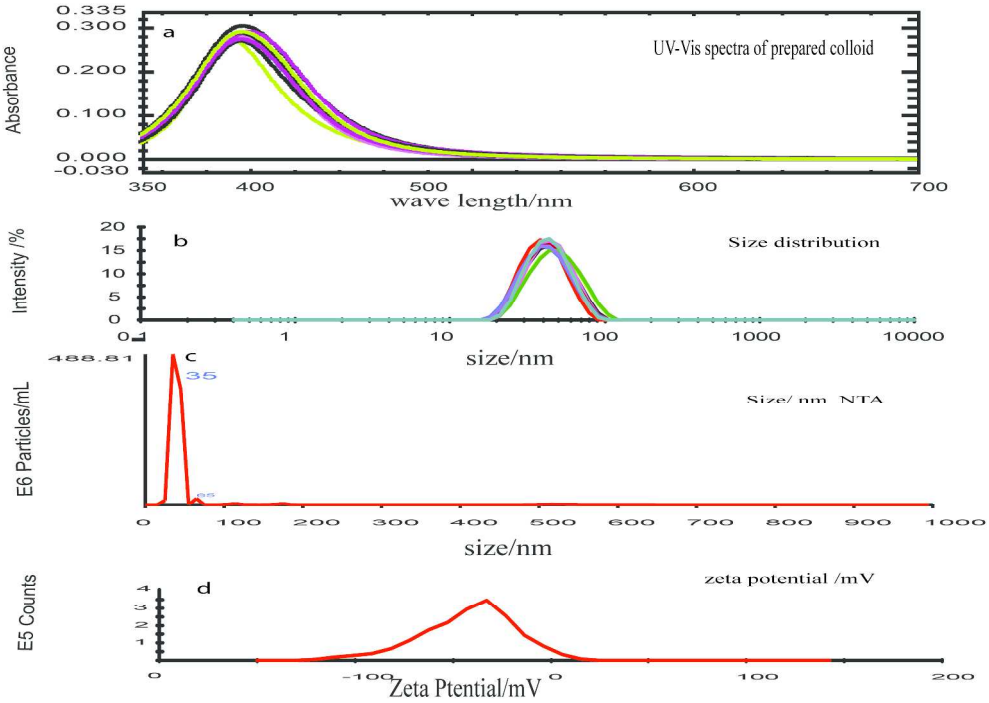

Characterisation of prepared nanoparticles, UV-Visible spectra, size distribution, size determination using NTA, and zeta potential as indicated in captions

297x210mm (300 x 300 DPI)

For Review

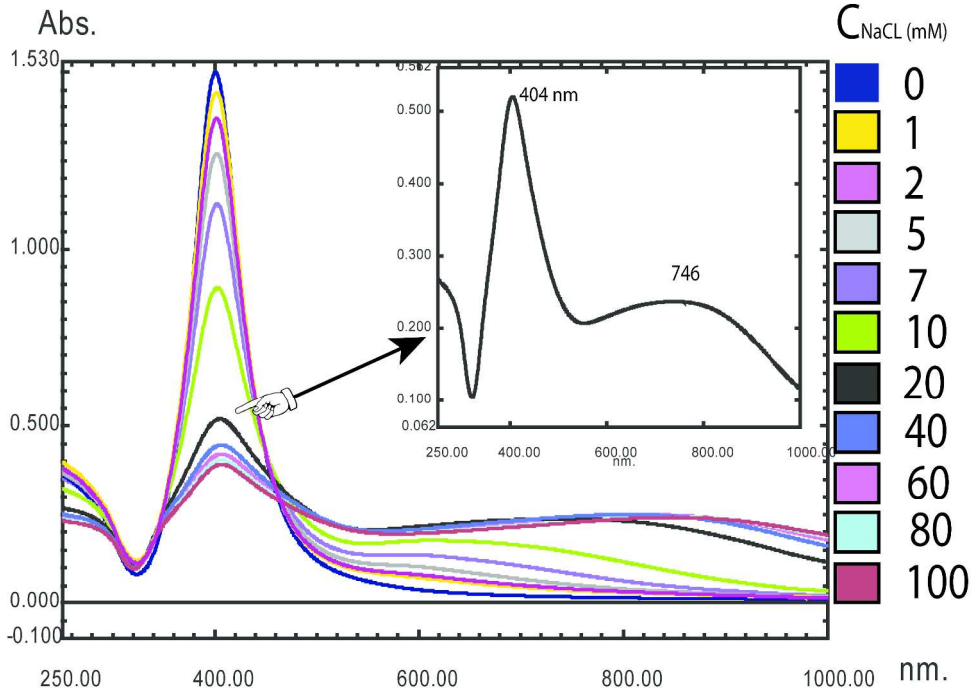

Effects of using diluted silver colloids with various concentrations of NaCl as indicated in legend on UV-Vis spectra (Surface Plasmon Resonance)

297x210mm (300 x 300 DPI)

For Review

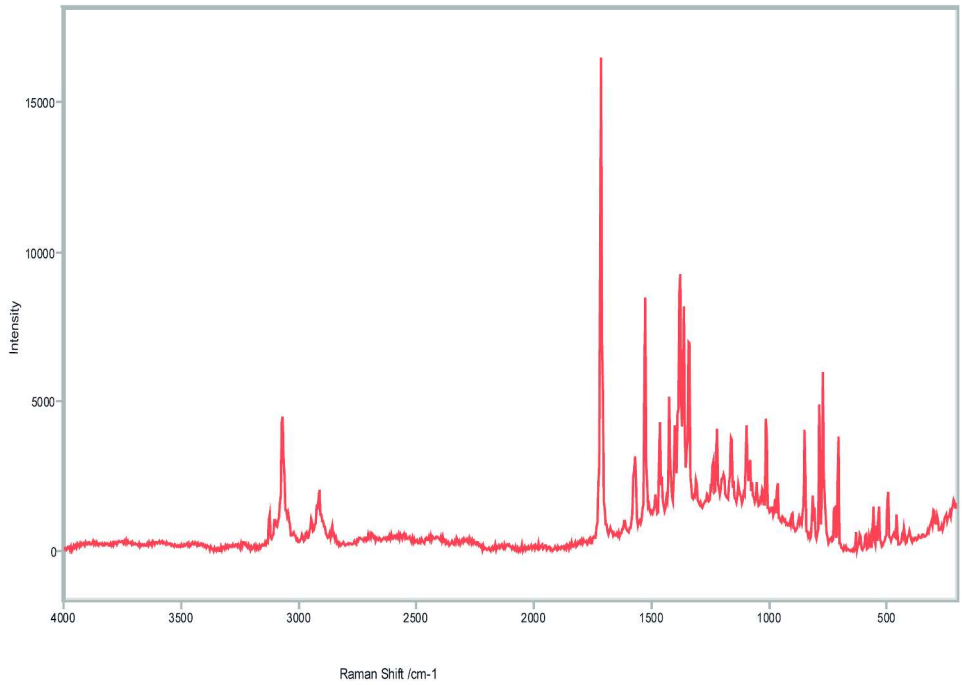

Experimental Raman spectrum collected at 532 nm excitation wavelength

297x210mm (300 x 300 DPI)

For Review

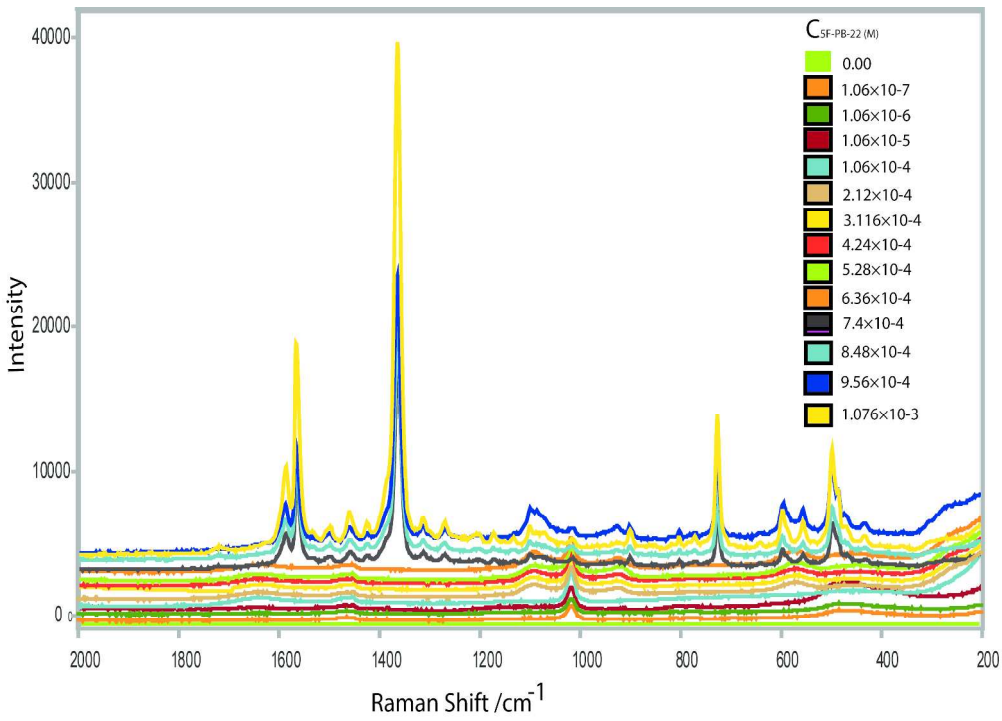

Effects of using diluted silver colloids with various concentrations of 5F-PB-22 as indicated in legend on SERS spectra (without using NaCl)

281x199mm (300 x 300 DPI)

For Review

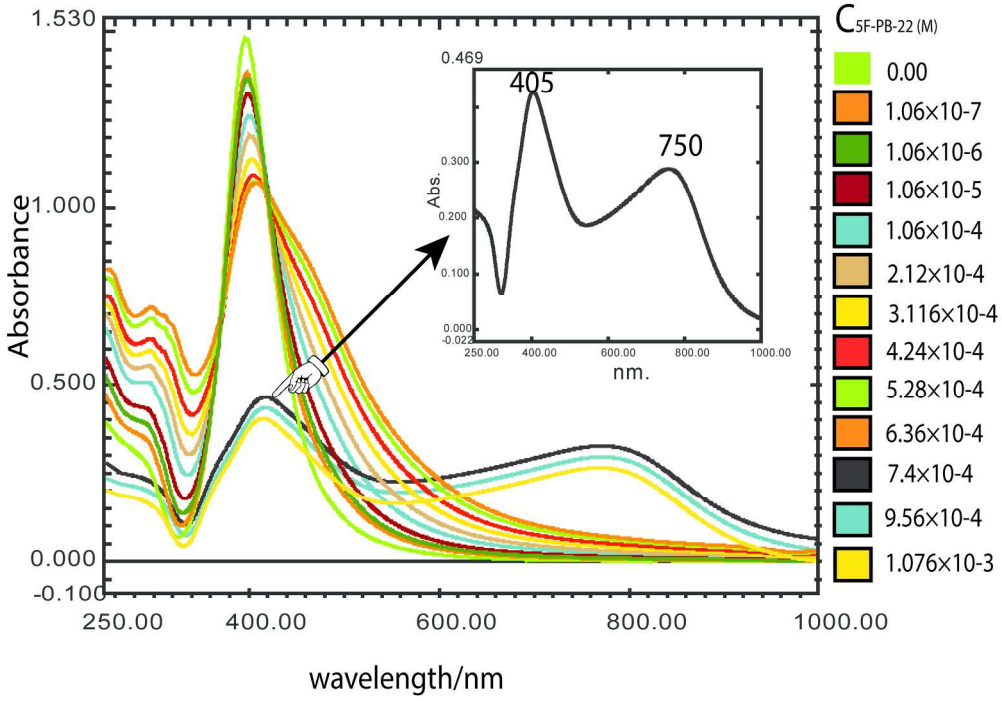

209x148mm (300 x 300 DPI)

For Review

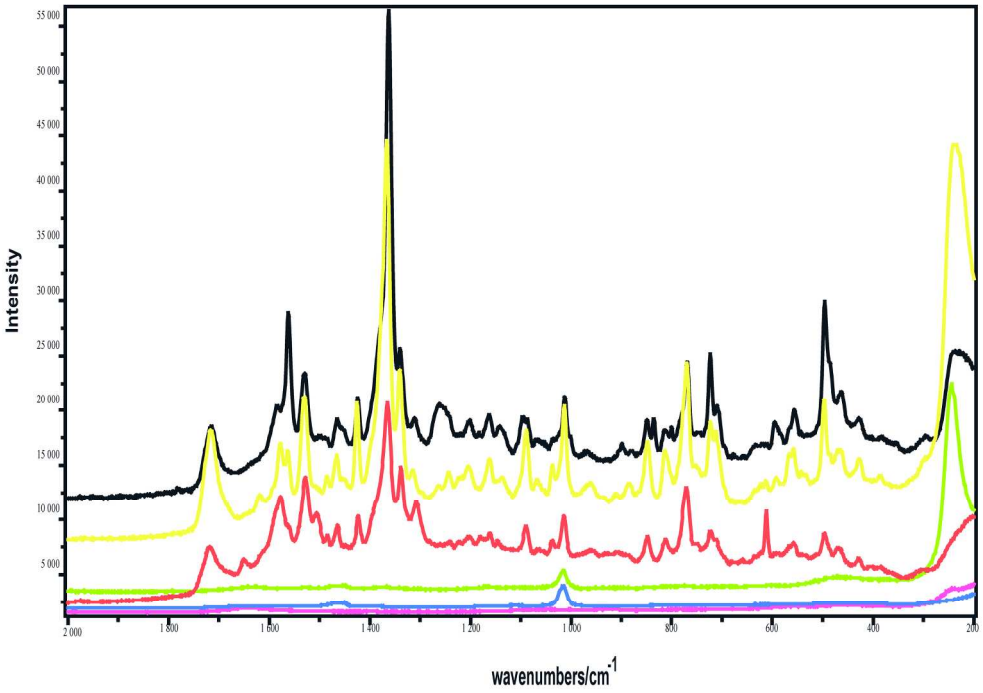

Raman, SERS spectra collected at 532nm from different sample preparation procedures ; pink line; background (diluted HPAg), Blue spectrum; 1.06× 10-7 M in diluted HPAg, green spectrum; 1.06× 10-7 M in diluted HPAg aggregated with 100mM NaCl, Black line; first spike 10mM NaCl, second spike to raise 5F-PB-22 to 1.06× 10-7 M, third spike 20 mM NaCl. Yellow line; first spike 10mM NaCl, second spike to raise 5F-PB-22 to 1.06× 10-7 M, third spike 40 mM NaCl. Red line; first spike 10mM NaCl, second spike to raise 5F-PB-22 to 2.12×10-8 M, third spike 20 mM NaCl

209x148mm (300 x 300 DPI)

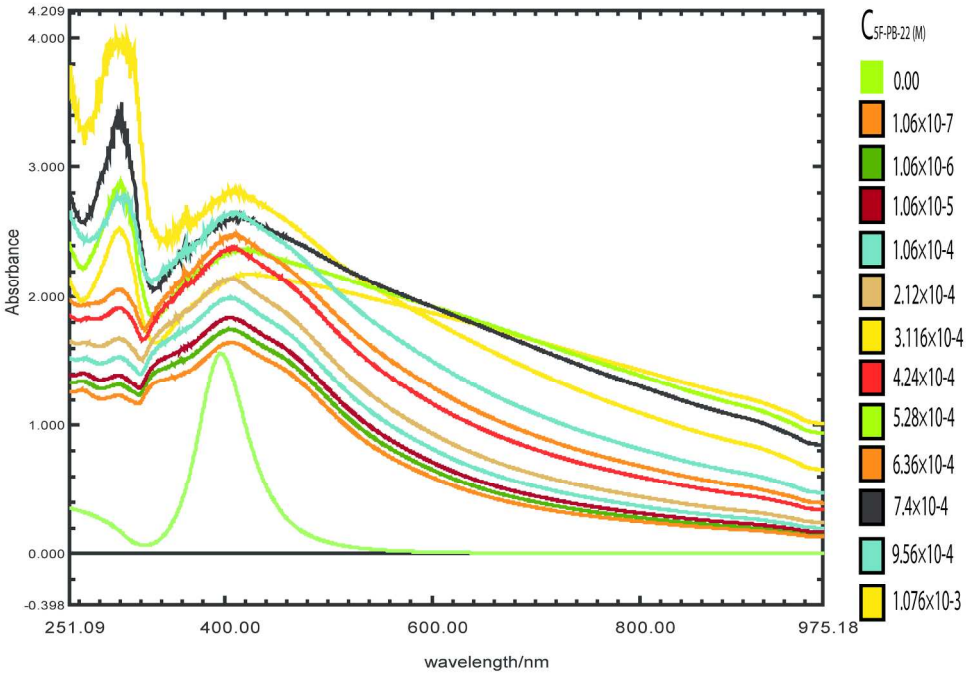

Effects of using 10mM NaCl pre-aggregated diluted silver colloids with various concentrations of 5F-PB-22 as indicated in legend on UV-Vis spectra (Surface Plasmon Resonance)

209x148mm (300 x 300 DPI)

For Review

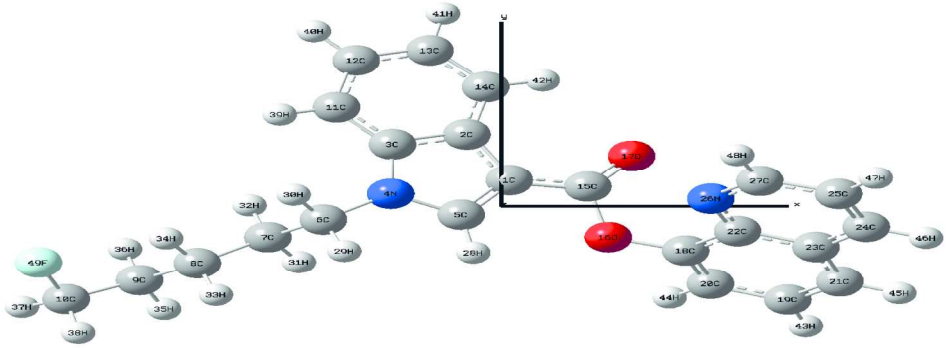

B3LYP 3-21 optimized molecular structure of the 5F-PB-22

209x148mm (300 x 300 DPI)

For Review

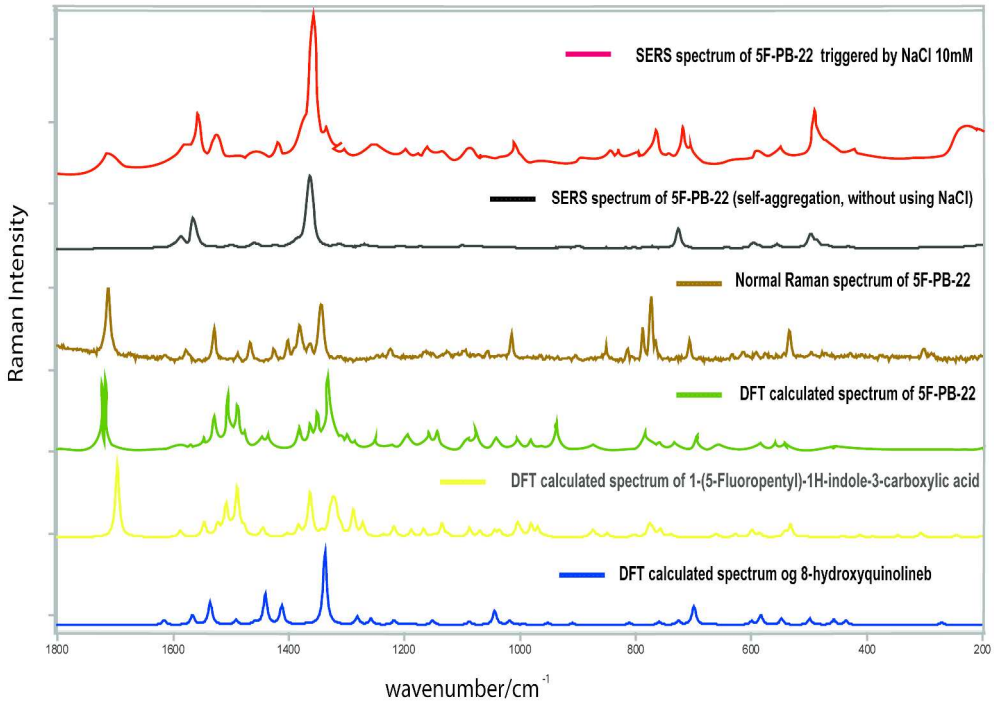

Experimental and DFT- calculated Raman spectra of 5F-PB-22, and its dissociation products as indicated in legend above each of spectra

297x210mm (300 x 300 DPI)

For Review

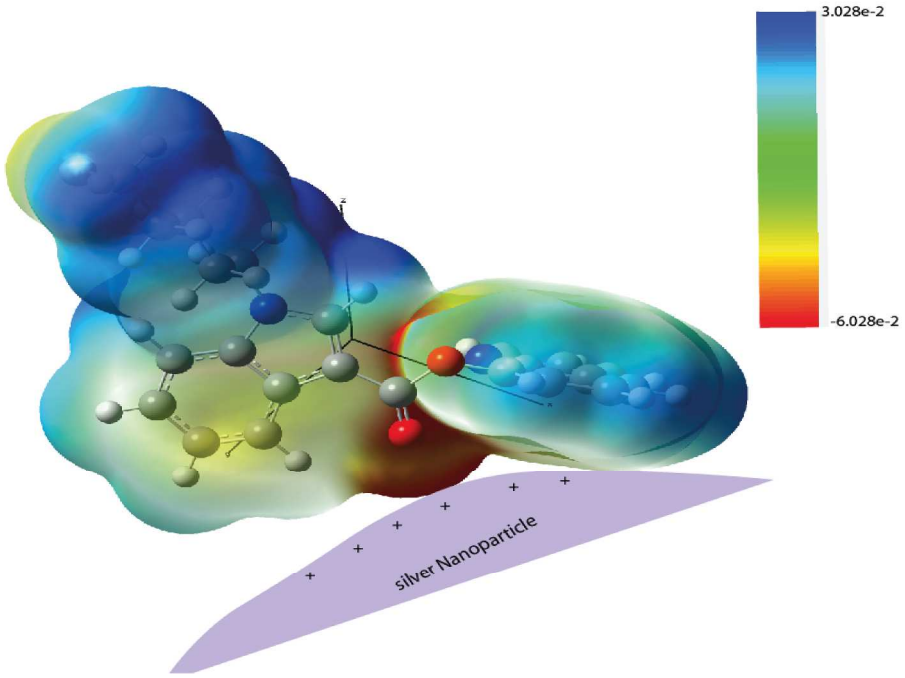

DFT calculated three-dimensional molecular electrostatic potentials in atomic units mapped on the electronic isosurface of 0.02 atomic unit

292x208mm (300 x 300 DPI)

For Review